LA-UR 89-275

(2)

Los Alamos National Laboratory is operated by the University of California for the United States Department of Energy under contract W-7405-ENG-36

TITLE: ONSET CONDITIONS FOR THE DRIVEN LOWER HYBRID DRIFT INSTABILITY IN AN EXPANDING MAGNETIZED PLASMA

AUTHOR(S): D. Winske, X-1

SUBMITTED TO: Report prepared for the Defense Nuclear Agency under Project Code RB, Task Code RC, Work Unit 167

Los Alamos National Laboratory
Los Alamos, New Mexico 87545

UNCLASSIFIED

SECURITY CLASSIFICATION OF THIS PAGE

REPORT DOCUMENTATION PAGE

1a. REPORT SECURITY CLASSIFICATION: UNCLASSIFIED	1b. RESTRICTIVE MARKINGS
2a. SECURITY CLASSIFICATION AUTHORITY	3. DISTRIBUTION / AVAILABILITY OF REPORT: Approved for public release, distribution unlimited
2b. DECLASSIFICATION / DOWNGRADING SCHEDULE	
4. PERFORMING ORGANIZATION REPORT NUMBER(S)	5. MONITORING ORGANIZATION REPORT NUMBER(S)
6a. NAME OF PERFORMING ORGANIZATION: Los Alamos National Laboratory; 6b. OFFICE SYMBOL (If applicable): X-1	7a. NAME OF MONITORING ORGANIZATION
6c. ADDRESS (City, State, and ZIP Code): Los Alamos, New Mexico 87545	7b. ADDRESS (City, State, and ZIP Code)
8a. NAME OF FUNDING / SPONSORING ORGANIZATION: Defense Nuclear Agency; 8b. OFFICE SYMBOL (If applicable): RAAE	9. PROCUREMENT INSTRUMENT IDENTIFICATION NUMBER
8c. ADDRESS (City, State, and ZIP Code): Washington DC 20305	10. SOURCE OF FUNDING NUMBERS: PROGRAM ELEMENT NO. / PROJECT NO. RB / TASK NO. RC / WORK UNIT ACCESSION NO. 167

11. TITLE (Include Security Classification)
ONSET CONDITIONS FOR THE DRIVEN LOWER HYBRID DRIFT INSTABILITY IN AN EXPANDING PLASMA

12. PERSONAL AUTHOR(S) D. Winske

13a. TYPE OF REPORT	13b. TIME COVERED	14. DATE OF REPORT (Year, Month, Day)	15. PAGE COUNT
Technical	FROM 10/88 TO 1/89	24 January 1989	31

16. SUPPLEMENTARY NOTATION
This work was supported by the Defense Nuclear Agency under Project Code RB, Task Code PC, Unit Work Code 167, Work Unit Title: Simulations and Modeling of HANE/VHANE

17 COSATI CODES		
FIELD	GROUP	SUB-GROUP

18. SUBJECT TERMS (Continue on reverse if necessary and identify by block number)
Laser experiment, Flute instabilities, Early time structuring, Numerical simulations.

19. ABSTRACT (Continue on reverse if necessary and identify by block number)

Conditions for the turn-on of short wavelength flute modes on plasmas expanding across an external magnetic field are discussed. The experimental data concerning scaling of the instability onset as a function of magnetic field are reviewed, followed by a similar review of numerical simulation results. Theoretical conditions for the appearance of the fast growing, short wavelength lower hybrid drift instability are derived. Overall, the experiments and simulations in which a scaling can be deduced suggest the turn-on of the instability is a strong function of the magnetic field. These results are discussed in relation to the NRL laser experiment, which in contrast exhibits little dependence of the instability onset on the applied field.

20. DISTRIBUTION / AVAILABILITY OF ABSTRACT: ☐ UNCLASSIFIED/UNLIMITED ☐ SAME AS RPT. ☐ DTIC USERS	21. ABSTRACT SECURITY CLASSIFICATION: UNCLASSIFIED
22a. NAME OF RESPONSIBLE INDIVIDUAL: Dan Winske	22b. TELEPHONE (Include Area Code): 505-667-2868; 22c. OFFICE SYMBOL: X-1

DD FORM 1473, 84 MAR — 83 APR edition may be used until exhausted. All other editions are obsolete.

SECURITY CLASSIFICATION OF THIS PAGE

UNCLASSIFIED

Onset Conditions for the Driven Lower Hybrid Drift Instability in an Expanding Magnetized Plasma

D. Winske

Applied Theoretical Physics Division

Los Alamos National Laboratory

Los Alamos, NM 87545

January 1989

Abstract

Conditions for the turn-on of short wavelength flute modes on plasmas expanding across an external magnetic field are discussed. The experimental data concerning scaling of the instability onset as a function of magnetic field are reviewed, followed by a similar review of numerical simulation results. Theoretical conditions for the appearance of the fast growing, short wavelength lower hybrid drift instability are derived. Overall, the experiments and simulations in which a scaling can be deduced suggest the turn-on of the instability is a strong function of the magnetic field. These results are discussed in relation to the NRL laser experiment, which in contrast exhibits little dependence of the instability onset on the applied field.

1. Introduction

Numerical experiments in which a plasma is created and then expands across an externally imposed magnetic field show that the surface becomes rippled, forming field aligned (flute) modes. Examples include gun generated plasmas [Dickinson *et al.*, 1962], laser produced plasmas [Okada *et al.*, 1981; Ripin *et al.*, 1987], and gas releases in space [Bernhardt *et al.*, 1987]. While these plasma have widely differing parameters (as described later), the fact that they exhibit similar behavior suggests a common instability mechanism. Numerous theoretical and simulation efforts have addressed the origin of these surface structures. Akimoto *et al.* [1988] summarize the recent experimental and theoretical work.

Presently, there is a general consensus concerning how the instability is produced. On the time and distance scales of interest, the ions are unmagnetized and expand outward from the source region unimpeded by the magnetic field, but constrained by the electrons that are tied to the field, via a radial electric field that is set up. The azimuthal $\vec{E} \times \vec{B}$ drift of the electrons relative to the ions is the free energy source for generating the unstable waves. Theoretically it is easily shown [e.g., Winske, 1988] that the range of instability extends from high frequency, fast growing ($\sim$ lower hybrid frequency), short wavelength (electron inertial length or shorter) modes to much longer wavelength ($\sim$ ion inertial scale), slower growing ($\sim$ ion cyclotron) waves. This range of scales has led to different approaches to derive the properties of the unstable waves and to different names given to the instability. Hassam and Huba [1987, 1988] start with a fluid approach including the Hall term and obtain the long wavelength limit of the instability, which they call the "unmagnetized ion Rayleigh-Taylor instability", while Winske [1988, 1989] and Galvez *et al.* [1988] employ

a kinetic treatment and concentrate on the short wavelength version of the instability, here called the "driven lower hybrid drift instability". Both approaches have a serious shortcoming, in that neither gives the correct scaling of the wavelength of the instability. The fluid approach includes the wavelength of the instability as a free parameter; the kinetic method predicts a wavelength corresponding to maximum growth that is consistent with simulations and some experiments, but is more than an order of magnitude shorter than that observed in other experiments [see Winske, 1989].

Leaving aside this unresolved issue of the wavelength, we turn to another question of interest at present, namely the scaling of the turn-on of the instability with parameters, particularly the applied magnetic field and the ion mass. Huba [1987] has shown that the long wavelength unmagnetized ion Rayleigh-Taylor instability has an onset condition that is independent of the magnetic field, which is in agreement with experiments carried out with the NRL laser. The issue at hand is what are the corresponding turn-on criteria for the driven lower hybrid drift instability, how do they scale with parameters, and what do they predict for the experiments. To facilitate the discussion, the rest of the report is broken up into four sections. Sections 2 and 3 review the relevant experiments and simulations, respectively, to infer possible onset criteria. Then, based in part on these results as well as the linear properties of the instability, turn-on conditions for the driven lower hybrid drift instability are derived in Section 4. Generally, the four onset conditions that are considered all show a rather strong dependence on the applied magnetic field, in contradiction to the laser experiments of Ripin *et al.* [1987]. These differences are discussed further in Section 5, where possible tests using experiments and simulations to resolve the discrepancy are proposed.

2. Review of Experiments

The results of four different experiments in which surface waves are observed are discussed: (A) the AMPTE barium releases in the magnetotail [Bernhardt *et al.*, 1987], (B) the plasmoid experiments of Dickinson *et al.* [1962], and laser generated plasma experiments of (C) Okada *et al.* [1981] and (D) Ripin *et al.* [1987].

A. Preliminaries

Before proceeding, we introduce a few basic concepts that will be used repeatedly throughout. The experimental arrangement we wish to consider is shown schematically in Figure 1. The initial conditions consist of a plasma source containing N ions and electrons with initial radius R_* expanding radially outward with velocity V_D into a low density background plasma (or vacuum) across a magnetic field of magnitude B. The expansion velocity V_D is assumed to be subAlfvenic and the initial plasma beta $\beta \gg 1$, so that as the plasma expands, it excludes the magnetic field and forms a diamagnetic cavity. The expansion continues out to the magnetic confinement radius, R_B, where the excluded magnetic field energy balances the initial kinetic energy of the expansion:

$$\frac{1}{2} N m_i V_D^2 = \frac{B^2}{8\pi} V \tag{1}$$

where V is the final volume ($V = 4\pi R_B^3/3$ in 3-D, $\pi R_B^2 L$ in 2-D).

The above simple argument assumes that the expansion is everywhere perpendicular to B. While this is a reasonably good approximation in 3-D, one can include the free expansion along B as well [Gisler and Lemons, 1988]. The convenient parameter to measure distance is R_B. However, because R_B changes with magnetic field strength, which is one of the parameters we wish to vary, we will imagine an experiment with reference parameters

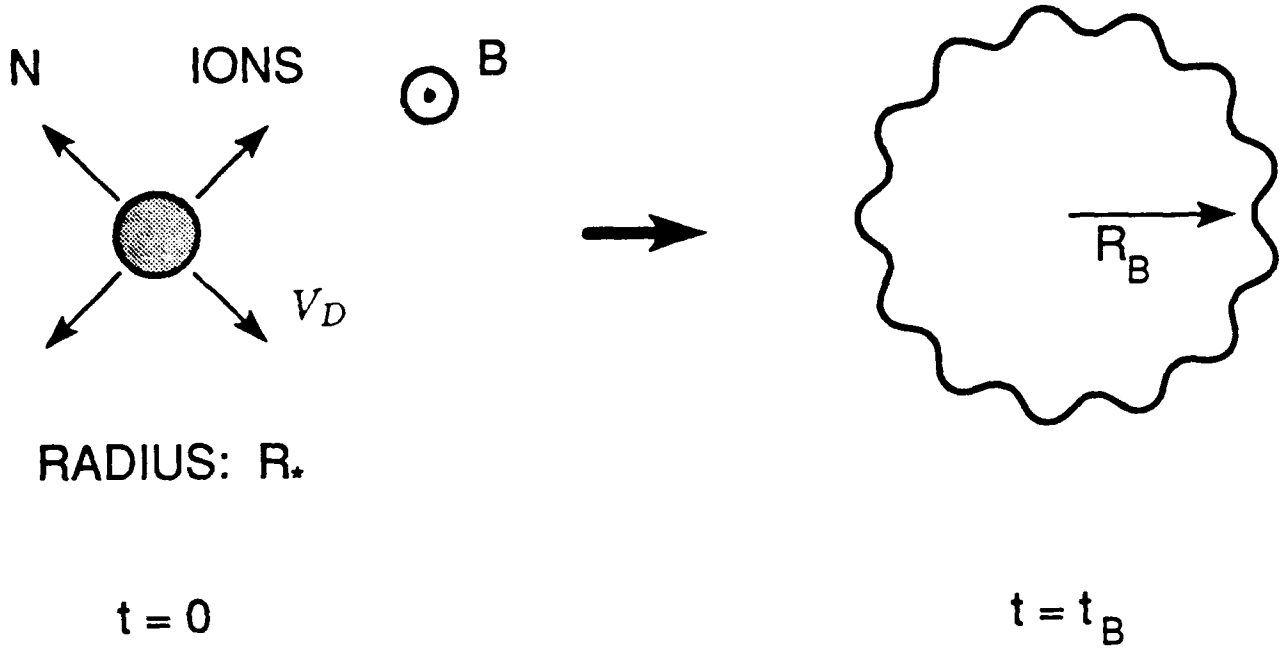

Figure 1. Schematic of plasma expansion experiments: N ions and electrons with initial radius R_* expanding into magnetic field B with velocity V_D; expansion stops with formation of diamagnetic cavity of radius R_B.

$B = B_o$ with corresponding $R_B = R_o$ and use those parameters as a basis for scaling studies. Similarly, scalings will be done with a reference ion mass, m_o, and one could carry out a comparable analysis for other initial parameters as well.

From the same dynamical considerations, one can show that the velocity as a function of times is

$$V(R) = V_D[1 - (R/R_B)^\alpha]^{1/2} \tag{2}$$

where $\alpha = 2$ (2-D) or 3(3-D). By integrating dR/V(R) from R=0 to $R = R_B$, one obtains the time corresponding to maximum expansion of the cloud

$$t_B = aR_B/V_D \tag{3}$$

where a=1.4 in 3-D, $\pi/2$ in 2-D. A third important parameter is ρ_i, the directed ion gyroradius

$$\rho_i = V_D/\Omega_i \tag{4}$$

where $\Omega_i = eB/m_ic$ = ion gyrofrequency. Our previous study [Winske, 1989] has suggested that ρ_i/R_B is the single most important parameter to characterize the strength of the driven lower hybrid drift instability.

B. AMPTE

The AMPTE (Active Magnetospheric Particle Tracers Explorers) mission [Krimigis *et al.*, 1982] involved a number of chemical releases in space, one of which occurred in March 1985 with the release of barium ions in the magnetotail. In this experiment about 10^{25} atoms were released with initial velocity $V_D \sim 1.3$km/sec into the hot magnetotail plasma and ambient magnetic field of about 8nT. Because of the finite ionization time for

the barium (about 30 sec) and the expansion of the cloud, the actual barium density is a complicated function of time. Nevertheless, ground based observations showed a maximum expansion radius, $R \sim 210$km, consistent with that calculated from (1), $R_B \sim 240$km, taking into account the free expansion along the magnetic field. Furthermore, for these parameters $\rho_i \sim 240$km as well. Of interest here are the optical observations of Bernhardt *et al.* [1987], who saw striations on the surface of the cloud starting at $t_c \simeq 180$sec, corresponding to $R_c < R_B$, which persisted beyond the time of maximum expansion, $t_B \simeq 240$sec, and the beginning of the recollapse of the cloud. From the optical images, it was determined that the mode number of the instability was m=24, which corresponds to a wavelength $\lambda \simeq 55$km, using the measured R=210km at maximum extension. The wavelength is considerable longer than that corresponding to the driven lower hybrid drift instability, as discussed recently by Winske [1989].

C. Plasmoid Experiments

The second set of experiments to be considered were carried out by Dickinson *et al.* [1962], in which a plasma was produced by directing a plasma gun against a copper barrier. The resulting plasma expands with velocity $V_D \sim 10^4$m/sec across a magnetic field that could be varied in strength from 0 to 0.8T. In this case the composition of the plasma is not known very well, although assuming it consisted of copper ions with charge state Z, one can compute $N \sim 10^{17}$ from the measured $R_B \simeq 1$cm (B=0.8T). Similarly, one infers that $\rho_i = 0.8Z$ cm. In these experiments flute modes were observed photographically on the expanding surface of the plasma and the position of the tips of the flutes and the edge of the main plasma column could be determined as a function of time. The results are shown in Figure 2, for various values of the applied magnetic field. Generally, one sees that the tips

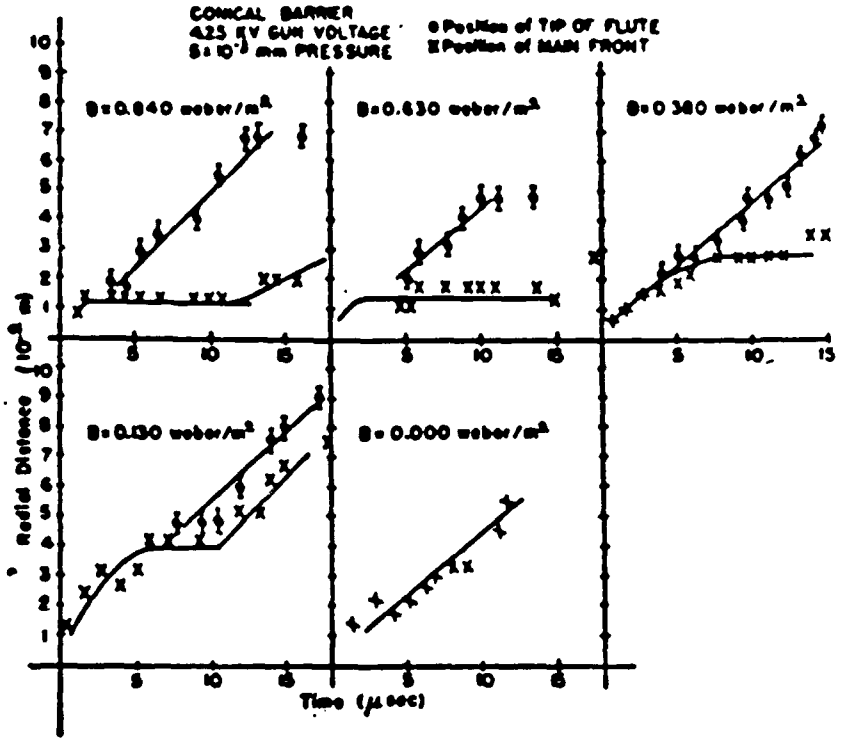

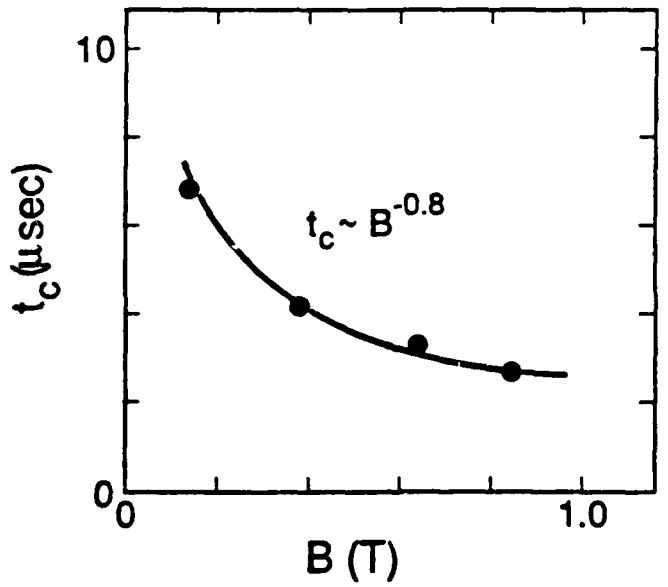

Figure 2. [top] Results from Dickinson *et al.* [1962] showing position of flute tips (circles) and plasma core surface (x's) versus time for various values of the applied magnetic field. [bottom] Onset time of instability (where flute and core curves cross) versus B.

the tips freestream outward, while the central core expands to some maximum radius R_B. If one plots the time (t_c) when the flutes and core become distinct by extrapolating the separate curves back until they cross, one finds (lower panel of Figure 2) that $t_c \sim B^{-0.8}$ and $R_c \sim R_B$. It is also interesting to note that other studies discussed in Dickinson *et al.* [1962] show that the wavelength of the instability, $\lambda \sim B^{-\alpha}, \alpha < 1$ (consistent with the driven lower hybrid drift instability [Okada *et al.*, 1981; Winske, 1988]) and $R_B \sim B^{-\delta}, \delta < 1$ (consistent with $R_B \sim B^{-2/3}$ in 3-D).

D. Japanese Laser Experiments

The next set of experiments involve a laser generated plasma expanding against a strong magnetic field, $B \sim$ 0.5-1.3T [Okada *et al.*, 1981]. A glass laser ($\sim$ 100 J) strikes an aluminum target, with the plasma expanding out to $R_B \sim$ 1-2cm, with $\rho_i \simeq R_B$. The flutes appear near $R_c \sim R_B$, but no studies of the onset of the instability with B were reported.

E. NRL Laser Experiments

The NRL laser experiments [Ripin *et al.*, 1987] are similar to the Japanese experiments in overall form, although the magnetic field was a little weaker (B=0.1-1.0T) and the plasma confinement radius was much larger, $R_B \sim 3-15$cm, with comparable ρ_i (assuming Al^{+10}). In this case, however, the instability appears well before the plasma reaches its maximum confinement radius. The panels at the top of Figure 3 show the position of the flutes (open circles) and plasma core (solid circles) as a function of time for two different magnetic field strengths. The points at different times, however, are from different laser shots, unlike the Dickinson *et al.* [1962] experiments shown earlier. However, similar to Dickinson *et al.*, the flutes freestream outward, while the plasma core comes to rest at

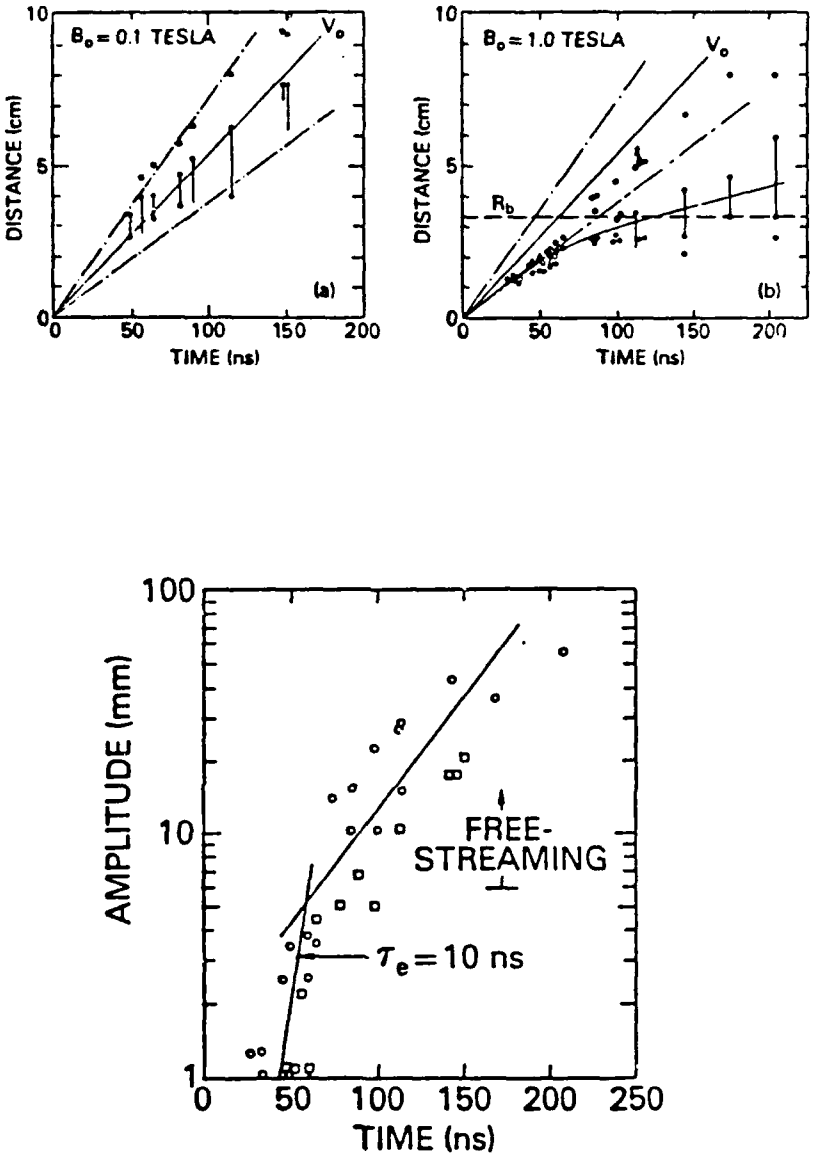

Figure 3. [top] Results from Ripin *et al.* [1987] showing position of flute tips (open circles) and plasma core surface (closed circles) at different times (from different shots). [bottom] Amplitude of flutes for both cases (squares=0.1T; circles=1.0T) at different times showing lack of B dependence on onset time.

$R = R_B$. For the weaker field case (B=0.1T), R_B is about 15 cm, off scale in the picture. The bottom panel of Figure 3 plots the data for the flutes for both magnetic field values (B=0.1T corresponds to the squares). Interestingly, the data suggests that the onset of the instability is independent of the magnetic field, contrary to that displayed in Figure 2.

F. Summary

In all four experiments a strong flute instability is observed. From the data one can raise two important issues. The first is where does the instability turn on. When R_B is large (AMPTE, NRL) the instability appears well before R_B. The other two situations (Dickinson, Okada) see the instability at $R_c \simeq R_B$; in these cases, however, R_B is only 1-2 cm and perhaps at these small distances the diagnostics cannot easily distinguish between R_c and R_B. The second issue is how does the turn-on of the instability depend on the applied magnetic field. One knows that there must be some dependence, as no instability is observed without the magnetic field being present [Dickinson *et al.*, 1962; Ripin *et al.*, 1987]. The results of Dickinson *et al.* [1962] further indicate (Figure 2) that the turn-on depends strongly on B, $t_c \sim B^{-0.8}$. However, it should be kept in mind that since $R_c \simeq R_B$ in that experiment, the turn-on time may just reflect the time to maximum expansion, $t_B \sim R_B \sim B^{-2/3}$. On the other hand, the experiments of Ripin *et al.* [1987] show little, if any, dependence on B. A closer examination of the bottom panel of Figure 3 shows that during the growth stage ($t < 60$ns) the circles (stronger field case) tend to lie to the left of the squares, which suggests some dependence on the field strength. Again, because the points come from different shots, it is difficult to draw any definitive conclusions from the figure. We thus turn to the simulations to look for further clues.

3. Review of Simulations

A number of simulations using different physics models have been carried out which show the development of flute modes on expanding plasmas. We review the relevant results of each, then summarize at the end. Further discussion of each of these calculations is found in Akimoto *et al.* [1988].

A. Hybrid Simulations with $m_e = 0$

Brecht and Thoms [1988] used a particle ion fluid electron hybrid code to study the instability in 2-D and 3-D. In these calculations ρ_i/R_B is much less than unity. The instability appears when $R_c \simeq R_B$ in 2-D and somewhat faster in 3-D. The shortest allowable modes in the simulation dominate. No scaling with B has been reported.

B. Hybrid Simulations with $m_e \neq 0$

Sgro *et al.* [1988] employed a hybrid model containing electron inertial effects. The calculations were done in a slab geometry, whith the plasma thus expanding in one direction. In these calculations the initial plasma state is characterized by $\rho_i/R_B \sim 1$ and $T_i \gg T_e$. The instability starts to develop before R_B, but the growth of the flutes is most dramatic when the plasma recompresses. Scaling with ion mass, but not B, was done. At higher m_i/m_e ratio the instability develops later in time, although it is difficult to infer an onset time scaling with ion mass.

C. MHD Code with Hall Term

Huba *et al.* [1987] show that the instability also occurs in a single fluid code, when the Hall term is included. (Without it, the usual Rayleigh-Taylor instability grows instead.) The simulations were carried out in a slab geometry by imposing an artificial gravity; R_B

is not clearly defined in this case. The instability grows rapidly, at the shortest allowable wavelength. No scaling studies have yet been done.

D. Electrostatic Particle Code

Galvez *et al.* [1988] consider a hot plasma cylinder ($R_c > \rho_i$), expanding thermally against a magnetic field in the electrostatic limit. Thus, no magnetic cavity forms and R_B is not a relevant parameter. It was noted in these simulations that it takes some time before the instability grows, as a charge layer is formed first. From the results of the simulations with various values of B, it is evident that there is some (weak) dependence on the magnetic field, with the instability developing sooner when B is stronger, although a scaling of t_c with B has not been extracted.

E. Electromagnetic Particle Simulations

Winske [1988] used a 2-D electromagnetic particle code to show the formation of the diamagnetic cavity and the growth of short wavelength flute modes. Figure 4 [from Winske (1989)] displays an example of one such calculation, showing ion density contours at various times. It is clear that the instability develops at $R_c < R_B$ and the flutes stay relatively small until the recollapse of the central core, when then become lengthened as the flutes continue to stream outward. The mode number also changes at this time, as discussed in more detail by Winske [1989]. Runs with various mass ratios and magnetic field strengths were also carried out. Figure 5 (again from [Winske, 1989]) shows that the observed wavenumbers during the growth stage (squares) are consistent with theory (solid lines) for the driven lower hybrid drift instability. Of more direct interest here is Figure 6, which shows the time when the instability appears as a function of applied magnetic field and ion mass, $t_c \sim B^{-1/2}(m_i/m_e)^{1/4}$. Calculations in 3-D [Barnes *et al.*, in preparation]

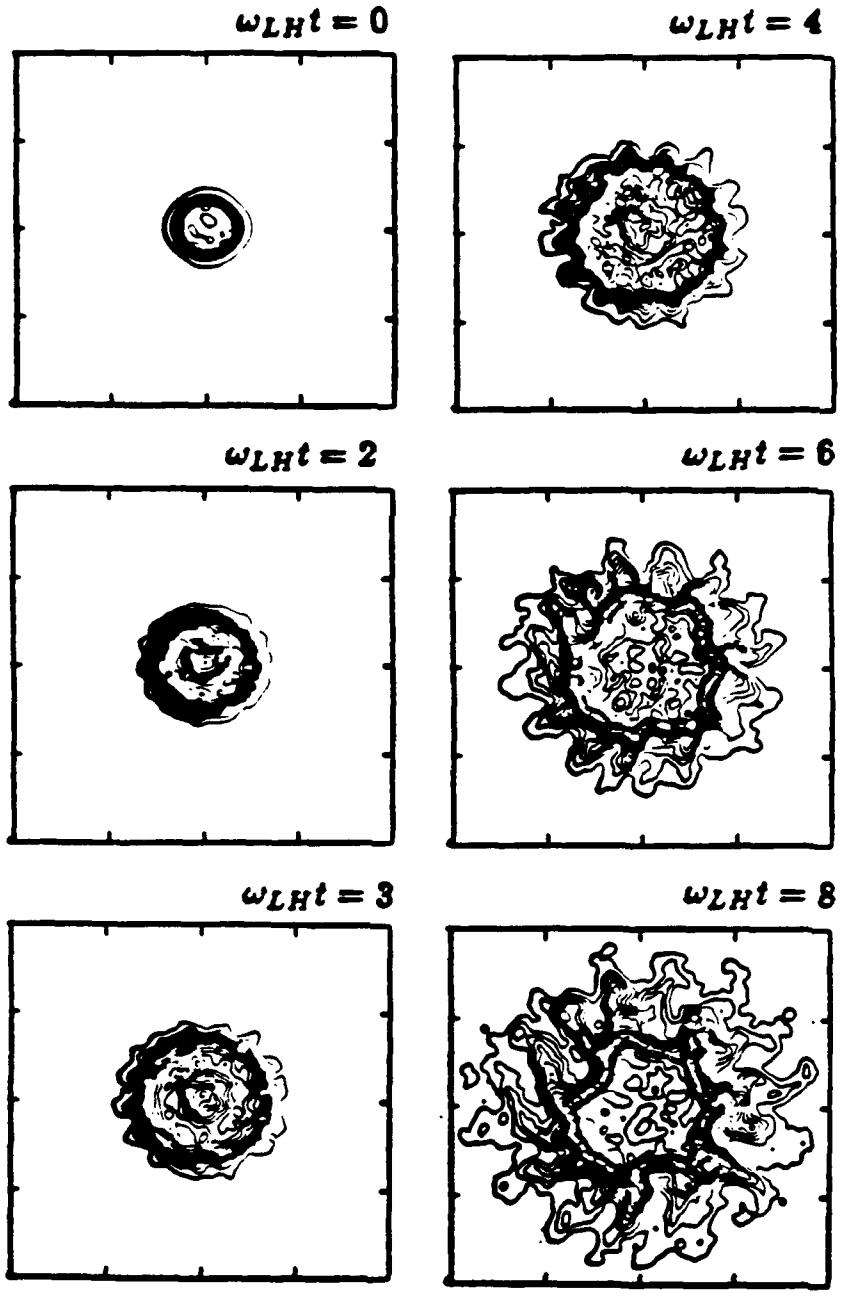

Figure 4. Results of particle simulations [Winske, 1989] displaying ion contours at various times to show the expansion of the plasma and development of the instability on the surface.

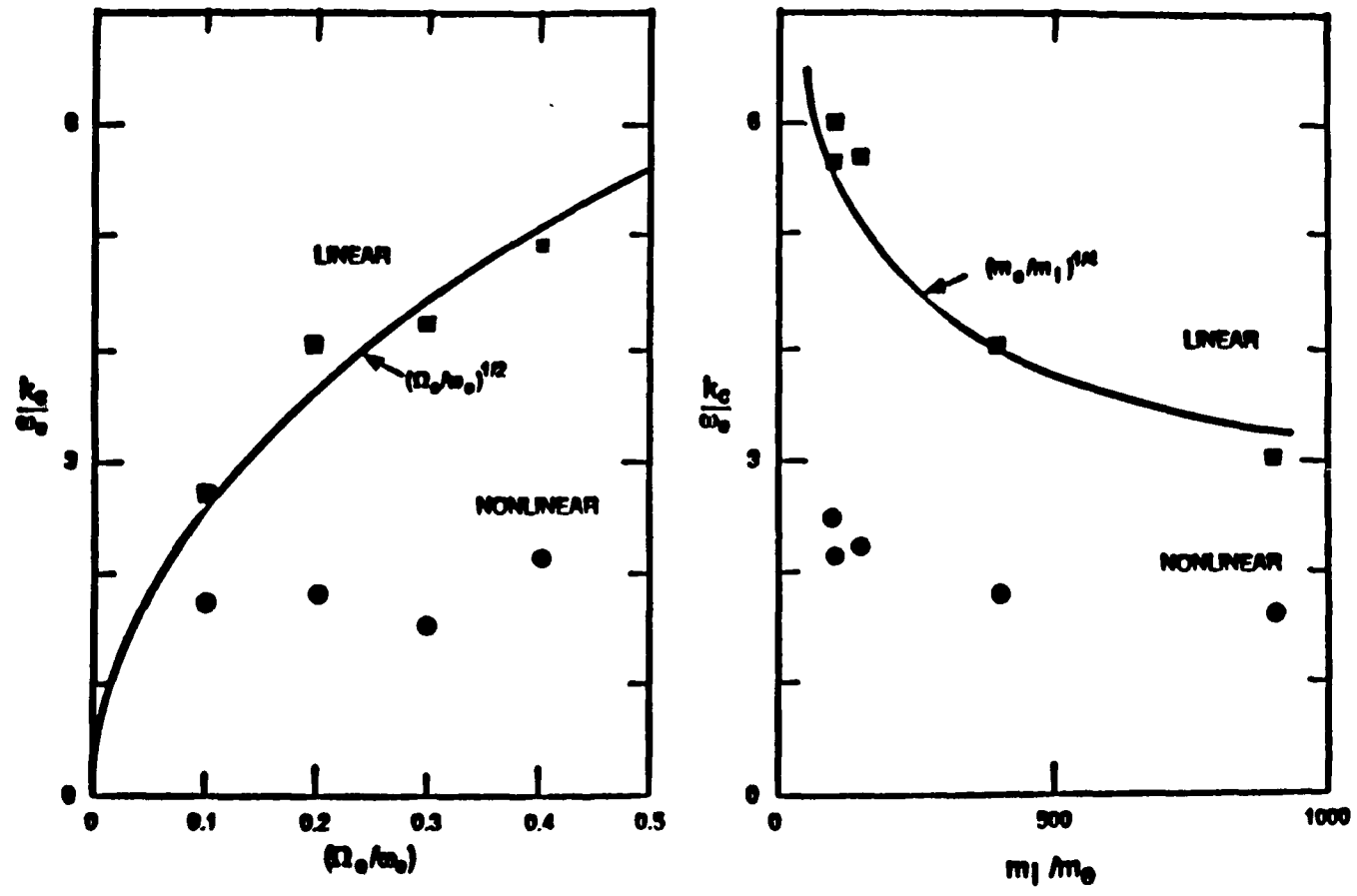

Figure 5. Results of particle simulations [Winske, 1989] showing dependence of wavenumber at early times (squares) during the growth phase and later (circles) during the recompression phase as a function of the magnetic field (expressed here as ω_e/Ω_e) and ion mass (m_i/m_e). Solid curves are theoretical results for the driven lower hybrid drift instability.

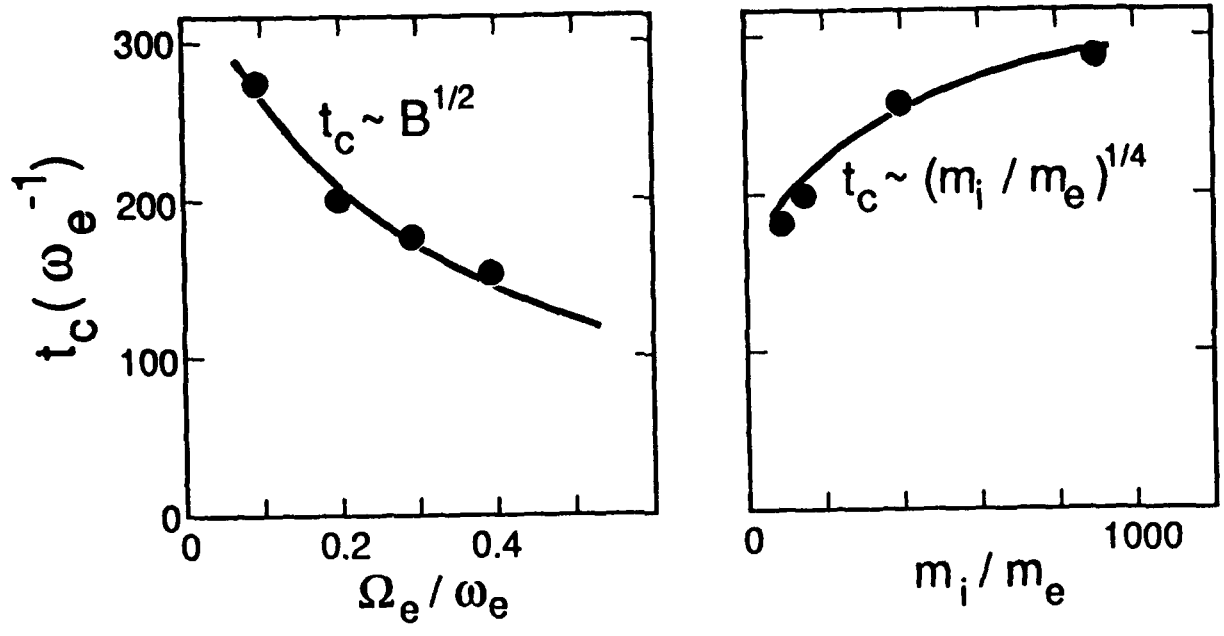

Figure 6. Results of the same simulations showing the onset time of the instability versus magnetic field strength and ion mass.

show similar behavior, and as with those of Brecht and Thomas [1988], indicate that the instability develops somewhat faster for comparable parameters, because the plasma deceleration is larger in 3-D.

F. Summary

The simulations show that the instability does develop, in a variety of physics models consistent with linear theory. In most of the simulations the instability turns on rapidly, i.e., $R_c < R_B$. They also demonstrate that the flutes do not become large until the core plasma slows enough to become well separated from the streaming flute tips. And the simulations suggest the onset of the instability decreases with magnetic field strength and increases with the ion to electron mass ratio. The one exception is the hybrid simulation of Brecht and Thomas [1988]. In their case, however, because $\rho_i \ll R_B$, the instability is very weak, compounded by the fact that because of the grid used in the simulations the wavelengths are long, $\lambda \sim c/\omega_i$ (ion plasma frequency $= \omega_i = (4\pi n_i e^2/m_i)^{1/2}$). Thus, the instability grows very slowly and only appears when $R_c \simeq R_B$, when the deceleration is largest.

However given these results, it is not clear whether the simulations can say anything about the actual turn-on radius R_c or turn-on time t_c in an experiment. This is due in part because the simulations start with an ideal plasma state that has a well defined shape and velocity distribution that leads to rapid growth of the instability. The initial conditions in the actual experiment are much more complex, because the plasma is generated by a laser (or gun) beam striking a target, or by a release of neutral atoms that ionize over a finite time interval. In addition, because of computational constraints, the initial radius of the plasma R_* is not very small in relation to R_c and R_B, rather $R_* \sim R_c < R_B$. A third

complication is the presence of a background plasma in the actual experiments, absent in most of the simulations. In the laser experiments, for example, the ionization level of the background may be a strong function of position [Brecht, private communication, 1988], which may affect the turn-on position.

4. Theoretical Scalings

A. Preliminaries

We consider the driven lower hybrid drift instability in the limit of cold ions, in which case the relative electron ion streaming is due solely to the deceleration of the ions by the magnetic field [Winske, 1988]. The deceleration g is defined as

$$g = -\frac{dV_{ir}}{dt} = \delta \frac{V_D^2}{R_B}(\frac{R}{R_B})^\alpha \tag{5}$$

where $\alpha = 1, \delta = 1$(2-D) or $\alpha = 2, \delta = 3/2$ (3-D); g thus increases with radius and is a maximum at $R = R_B$. The above expression assumes an expansion perpendicular to B; in 3-D one can also include the free expansion along the magnetic field, which changes $\delta \rightarrow 2.3$ [Gisler and Lemons, 1988].

The corresponding cross-field drift is

$$V_g = g/\Omega_i \tag{6}$$

and the actual quantity of interest is V_g/v_A, where v_A is the Alfven speed, $v_A^2 = B^2/4\pi n m_i$ (v_A is a function of R, because the density n is).

We assume two different models for n(R). First, the plasma expands as a uniform cylinder:

$$N = n_* R_*^2 L\pi = n(R) R^2 L\pi \tag{7}$$

where n_*, R_* are the initial density and radius respectively. Second, the plasma compresses into a thin shell Δ, such that $n(R)$ =constant, i.e.,

$$N = n(R)2\pi R\Delta L \Rightarrow \Delta \sim 1/R \tag{8}$$

The first model implies

$$V_g/v_A = \rho_i/R_B = \text{constant} \quad (2-\text{D}) \tag{9}$$

and

$$V_g/v_A = \frac{3}{2}(\frac{R}{R_B})^{1/2}\frac{\rho_i}{R_B} \quad (3-\text{D}) \tag{10}$$

while the second yields (in 2-D)

$$V_g/v_A = (R/R_B)(\rho_i/R_B) \tag{11}$$

i.e., V_g/v_A increases linearly with R. In 3-D, this same model gives

$$V_g/v_A = \frac{3}{2}(R/R_B)^2(\rho_i/R_B) \tag{12}$$

Results of 2-D particle simulations [Winske, 1988] in which V_g/v_A is measured at various R shows behavior consistent with (11) (Figure 7).

B. Onset Criteria

We consider four different criteria for the turn-on of the instability, deriving each for one particular model [2-D expansion, n(R)=constant]. The following subsection summarizes the results for all the models.

The first criterion is that the instability turns on when

$$V_g/v_A \geq 2 \tag{13}$$

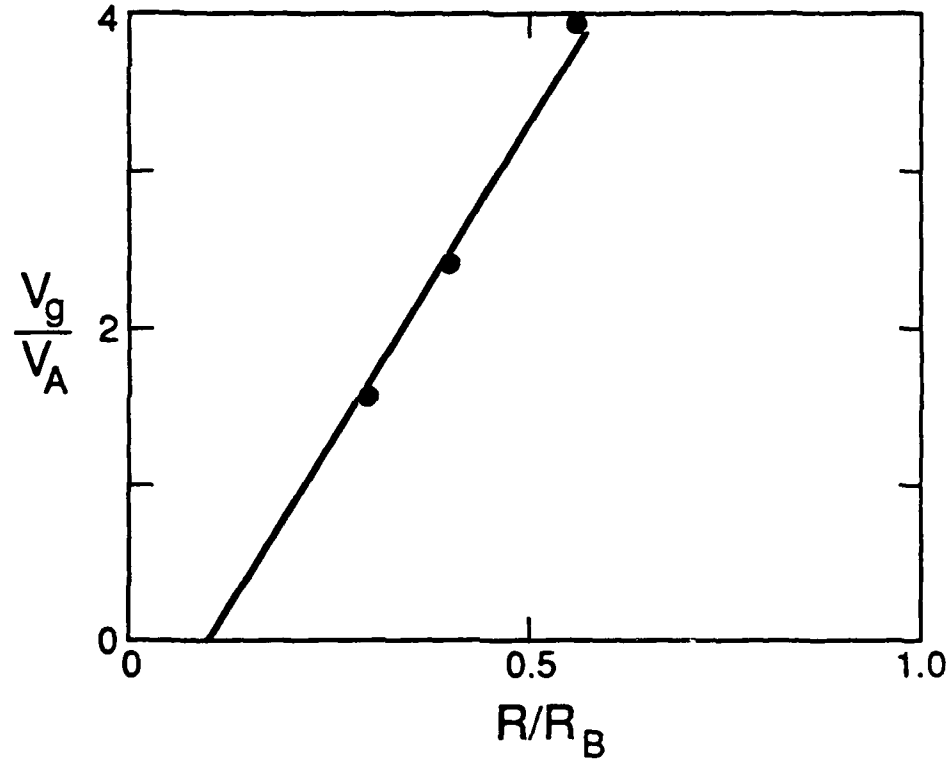

Figure 7. Results of particle simulations [Winske, 1988] showing the increase of V_g/v_A with radius R, suggesting $V_g/v_A \sim R$, consistent with (11).

When the ions are hot ($\beta_i \sim 1 \Rightarrow v_A \sim v_i$), (13) corresponds to $V_g > v_i$, the nonresonant regime of the lower hybrid drift instability. The condition (13) is also analogous to the one derived by Huba [1987] for the unmagnetized ion Rayleigh Taylor instability. In that case, the assumption of unmagnetized ions implies $\gamma > \Omega_i$. Hassam and Huba [1987] show that

$$\gamma = k(g/\epsilon_n)^{1/2} \tag{14}$$

where k is the wavenumber and $\epsilon_n = n^{-1}dn/dx$ is the density inverse scale length. Because $g \sim R_B^{-3} \sim B^2$, the righthand side of (14) is proportional to B and the expression $\gamma > \Omega_i$ is independent of B.

Our criterion is based on the results of Figure 8, showing the growth rate maximized over k and the corresponding wavenumber versus V_g/v_A ($T_e = 0, \beta_i = 10^{-4}, \epsilon_n c/\omega_i = 10$). For $V_g/v_A \leq 2$, both γ and k change rapidly, while for $V_g/v_A \geq 2$, they vary much more slowly. The condition (13) can thus be written as

$$\frac{V_g}{v_A} = \frac{R}{R_B}\frac{\rho_i}{R_B} > 2 \tag{15}$$

or

$$R_c > 2R_B/(\rho_i/R_B) \tag{16}$$

Normalizing to the reference case where $B = B_o$, $R_B = R_o$, $m_i = m_o$ and using the fact $R_B/R_o \sim (B_o/B)(m_i/m_o)^{1/2}$, $\rho_i/\rho_o = (B_o/B)(m_i/m_o)$ [in 2-D, from Eq. (1-3)]

$$\frac{R_c}{R_o} > \frac{B_o}{B}\frac{2}{(\rho_o/R_o)} \tag{17}$$

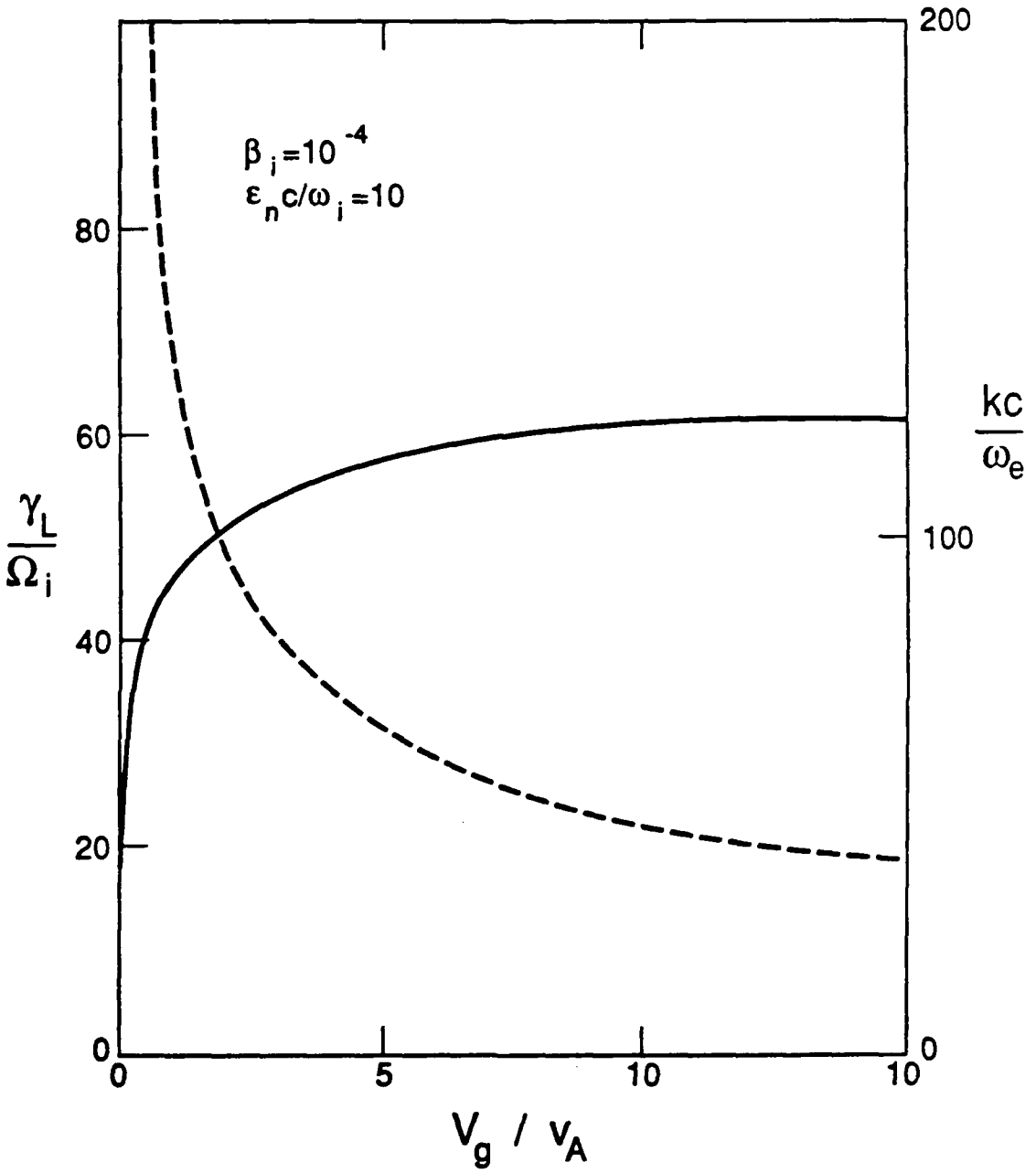

Figure 8. Results of linear theory for the driven lower hybrid drift instability showing the growth rate maximimized over wavenumber and the corresponding k versus V_g/v_A ($\beta_i = 10^{-4}, \epsilon_n c/\omega_i = 10$).

The second criterion is based on the linear growth rate. The waves grow from noise starting at $R = R_1$ and are seen when they reach a given size

$$h = \text{ height of flute } = \delta h e^{\gamma t} \tag{18}$$

where δh is the initial perturbation (noise). But $t \sim R/V_D$ and $\gamma \sim \omega_{LH}$ [lower hybrid frequency $= \omega_{LH} \simeq \Omega_i (m_i/m_e)^{1/2}$] so

$$R_c = \frac{V_D}{\omega_{LH}} \ln(h/\delta h) \tag{19}$$

or

$$\frac{R_c}{R_o} \sim \frac{B_o}{B} (\frac{m_i}{m_o})^{1/2} \tag{20}$$

The third turn-on condition is based on the fact that because the initial density of the cloud is so large the electron thermal beta, $\beta_e = 8\pi n_e T_e / B^2$, is much greater than unity. Because the driven lower hybrid drift instability is stabilized by β_e effects [Drake *et al.*, 1983], the instability turns on when β_e drops to some low value, ~ 1:

$$\beta_e = \frac{8\pi n_e T_e}{B^2} \leq 1 \tag{21}$$

If n_e =constant, because of compression of the cloud into a thin shell, β_e =constant and this condition does not apply. On the other hand, if we use the other model, $n(R) \sim R^{-2}$ (21) becomes

$$\frac{R_c}{R_o} = \sqrt{\beta_o} \frac{B_o}{B} \tag{22}$$

where $\beta_o = \beta_e(R_o)$.

The last criterion for instability onset is again based on Figure 8, which shows that for large V_g/v_A, k does not change very rapidly. As the plasma radius R increases, V_g/v_A

increases so that k decreases. It is assumed that the instability will grow when the mode number (m=kR) changes slowly in one growth time. Figure 8 (and the linear analysis in [Winske, 1988]) indicate that for $V_g/v_A > 1$,

$$kc/\omega_e \sim (V_g/v_A)^{-1/3} \tag{23}$$

so that

$$m = kR = \frac{Rn(R)^{1/2}}{(V_g/v_A)^{1/3}} \sim R^{2/3} \tag{24}$$

using (11). Thus

$$\Delta m/m \sim \Delta R/R \tag{25}$$

and

$$\Delta R \sim V(R)\Delta t \simeq V_D(1 - R^2/R_B^2)^{1/2}\Delta t \tag{26}$$

Taking $\Delta t \sim \gamma^{-1} \sim \omega_{LH}^{-1}$, we thus find

$$\frac{\Delta m}{m} \simeq \frac{\rho_i}{R_B}\frac{(1 - R^2/R_B^2)^{1/2}}{R/R_B}(\frac{m_e}{m_i})^{1/2} < q \tag{27}$$

where q is some small number, e.g., 0.1. Then one can easily show that R/R_B is small so that $(1 - R^2/R_B^2)^{1/2}$ can be neglected, yielding

$$\frac{R_c}{R_o} > \frac{1}{q}(\frac{m_e}{m_o})^{1/2}(\frac{m_i}{m_o})^{1/2}\frac{\rho_o}{R_o}\frac{B_o}{B} \tag{28}$$

C. Results for All Models

The results for both density models [Model 1: $n(R) \sim R^{-\alpha}$ ($\alpha = 2$ (2-D) or 3(3-D)) or Model 2: $n(R)$ ~constant] in both 2-D and 3-D are summarized in the following table. We express the scaling with magnetic field and ion mass in the following form:

$$\frac{R}{R_c} \sim (\frac{B}{B_o})^{\beta}(\frac{m_i}{m_o})^{\mu} \tag{29}$$

	2-D		3-D	
Criterion #	Model 1	Model 2	Model 1	Model 2
1	– –	$\beta = -1$	$\beta = -1/3$	$\beta = -1/2$
		$\mu = 0$	$\mu = -1/3$	$\mu = 0$
2	$\beta = -1$	$\beta = -1$	$\beta = -1$	$\beta = -1$
	$\mu = 1/2$	$\mu = 1/2$	$\mu = 1/2$	$\mu = 1/2$
3	$\beta = -1$	– –	$\beta = -2/3$	– –
	$\mu = 0$		$\mu = 0$	
4	– –	$\beta = -1$	$\beta = -1$	$\beta = -1$
		$\mu = 1/2$	$\mu = 1/2$	$\mu = 1/2$

D. Interpretation

We interpret the results displayed in the above table as follows. Conditions 2 and 4 essentially depend on the linear growth rate, $\gamma \sim \omega_{LH}$, and not on the density model assumed. So for all four models when these two conditions apply, one has $R/R_c \sim \omega_{LH}^{-1} \sim (B/B_o)^{-1}(m_i/m_o)^{1/2}$. The third condition depends on β_e, hence has no dependence on ion mass; when the density does not vary with radius, neither does β_e, and this condition is not applicable. Only the first turn-on condition shows significant model variation of the B and m_i dependence, and displays the weakest B dependence in 3-D. None of the 2-D conditions show the same scaling as seen in the 2-D simulations [Figure 6]. The fact that the simulation scaling is consistent with $\omega_{LH}^{-\alpha}$, with $\alpha \sim 1/2$, could suggest that conditions 2 or 4 may be applicable, but that the asymptotic value of the growth rate ($\gamma = \omega_{LH}$) is not quite correct. None of the criteria derived here have no dependence on the applied

magnetic field, as observed by Ripin *et al.* [1987], although the dependence in one case is fairly weak (Condition 1, Model 1 in 3-D). We will discuss these results further in relation to the experiments next.

5. Discussion

Previously, we have argued that the fluting which appears on the surface of plasma clouds expanding across an ambient magnetic field is due to the driven lower hybrid drift instability [Winske, 1988]. Because this is a high frequency short wavelength mode, to explain some of the observable manifestations of the instability, nonlinear effects need to be invoked [Winske, 1989]. In this report we have considered conditions for the turn-on of the instability deduced from linear theory and apply them to various numerical simulations and experiments in which the instability is excited. Four different onset conditions have been derived, and each has been worked out for both 2-D and 3-D expansions assuming two different models for the plasma density profile. This range of models has been considered in order to see if there is much sensitivity of the magnetic field and ion mass dependence on the model used. In addition, the various simulations and experiments tend to lie in different parameter regimes, and thus we do not expect all the data to be explained by a single scaling law.

Generally, the simulations are easier to understand. This is because the initial conditions are well known and one can (in principle) determine local quantities, such as drift velocities, density gradients, temperatures, etc., as needed by the theory. In addition, the simulations are free of complications such as changing charge states, impurities, radiation, background ionization effects, etc. The simulations in which scaling of the instability onset

has been attempted show faster turn-on with stronger magnetic field and smaller ion to electron mass ratio. These same trends are predicted for the linear growth rate of the instability. Thus, the simplest consistent explanation is that the onset time t_c scales as the inverse growth rate, γ^{-1}. That the simulations do not follow a simple scaling like (29) with $\beta = -1$ and $\mu = 1/2$ just reflects the fact that the growth rate used in those expressions ($\gamma \simeq \omega_{LH}$) is the idealized limit. Of course, it should also be kept in mind that the initial conditions in the simulation are chosen to promote rapid growth of the instability.

The experiments, however, are more ambiguous. From the published data of the plasma gun experiment of Dickinson *et al.* [1962] one can derive an onset time that scales inversely with B, $t_c \sim B^{-0.8}$. One possible explanation is that in this experiment the instability is strongly driven, given the large flutes that are observed, i.e., $\rho_i/R_B > 1$. The strong dependence on B then reflects the large linear growth rate, $\gamma \sim \omega_{LH}$. But assuming a copper plasma and B=0.8T, one readily computes $\omega_{LH}^{-1} \sim 2$ns (assuming Z=1). Because the experimental onset time at B=0.8T is about 1.2μsec, this implies about 10^3 e-folding times. Obviously, there is plenty of time for short wavelength modes to grow, saturate, and nonlinearly evolve into the structures actually seen. Alternatively, some mechanism such as finite β_e effects prevents the instability from growing until much later, $t \sim 1\mu$sec. Another possibility, already mentioned, is that the t_c scaling reflects the fact that the instability onset occurs near R_B, hence $t_c \sim t_B \sim R_B \sim B^{-2/3}$.

In the AMPTE experiment, on the other hand, one does not have the problem of trying to decipher a 25 year old experiment, but as there were only two magnetotail barium releases, one does not have a scaling for the onset of the instability. However, one is again faced with the fact that the onset time $\sim$ 180sec is much greater than $\omega_{LH}^{-1} \sim 2$

sec, suggesting the instability is inhibited from growing at early times. This could be due to the fact that the plasma beta is initially very large and the background plasma is hot, so that finite β_e effects can be used to explain the slow onset. Or again, because of the large discrepancy between the observed waves and those predicted for the driven lower hybrid drift instability, it is conceivable that the short wavelength modes have grown up and saturated and one is seeing the slower growing, nonlinear manifestation of the instability (in which case the onset criteria derived here are probably not relevant).

That leaves the laser experiments, especially the experiments of Ripin *et al.* [1987] in which the onset time was found to be independent of B. For Al^{+10} in a 0.1T magnetic field, one finds $\omega_{LH}^{-1} = 4\text{ns}$ compared to $t_c \approx 50\text{ns}$. There are many e-foldings possible (and many more for the 1.0T field case), again suggesting some initial inhibition of the instability (which could be finite β_e or complications due to the changing charge state of the aluminum or the background plasma conditions). Because the experiment is still operational, it suggests some further avenues of investigation to help clarify the onset question. With the improved capability to obtain multiple exposures per shot, it would be most useful to again check the B dependence of the onset time, to see if some, even weak, dependence on the magnetic field exists. Some of the theoretical onset conditions predict weaker magnetic field dependence in a realistic three dimensional expansion compared to the two dimensional simulations. A second set of useful experiments would be to vary the target material to test the mass scaling. No dependence on the ion mass could indicate that finite electron beta effects inhibit the instability growth at early times. A weak dependence on mass, particularly if opposite to a slightly stronger dependence on B, could suggest a growth rate type of scaling similar to that seen in the simulations. A final useful addition

to the experiment would be a more thorough study of the data from the electrostatic probe that detects the growth of the very short wavelength high frequency noise. Scaling of that noise with B and m_i could show that lower hybrid modes are indeed present and suggest that the actually observed waves are a nonlinear evolution of these shorter wavelength modes.

As a final note, it should be mentioned that not all of the burden falls on the experimenters. The simulators should also direct their efforts toward making the numerical calculations more realistic, i.e., including 3-D effects, improving the initial conditions of the plasma, and modeling some of the messier details (charge states, incompletely ionized background) of the laser experiment to assess how important a role they play.

Acknowledgements

We acknowledge useful and stimulating discussions with Drs. S. H. Brecht and V. A. Thomas. This work was performed under the auspices of the U. S. Department of Energy, and was supported by the Defense Nuclear Agency under Project Code RB, Task Code RC, Work Unit Code 167, and Work Unit Title "Simulations and Modeling of HANE/VHANE."

References

Akimoto, K., M. Galvez, S. P. Gary, A. G. Sgro, and D. Winske, Prompt structuring of a plasma expanding in an external magnetic field, *J. Geomag. Geoelect., 40*, 1161, 1988.

Bernhardt, P. A., R. A. Roussel-Dupre, M. B. Pongratz, G. Haerendel, A. Valenzuela, D. A. Gurnett, and R. R. Anderson, Observations and theory of the AMPTE magnetotail barium releases, *J. Geophys. Res., 92*, 5777, 1987.

Brecht, S. H., and V. A. Thomas, Multidimensional simulations using hybrid particle codes, *Comput. Phys. Comm., 48*, 135, 1988.

Dickinson, H., W. H. Bostick, J. N. DiMarco, and S. Koslov, Experimental study of Rayleigh Taylor instability in plasma, *Phys. Fluids, 5*, 1048, 1962.

Drake, J. F., J. D. Huba, and N. T. Gladd, "Stabilization" of the lower hybrid drift instability in finite beta plasmas, *Phys. Fluids, 26*, 2247, 1983.

Galvez, M., S. P. Gary, C. Barnes, and D. Winske, Computer simulations of plasma expansion across a magnetic field, *Phys. Fluids, 31*, 1554, 1988.

Gisler, G., and D. S. Lemons, Dynamics of a plasma expanding into a uniform magnetic field, *J. Geophys. Res.*, submitted, 1988.

Hassam, A. B., and J. D. Huba, Structuring in the AMPTE magnetotail barium releases, *Geophys. Res. Lett., 14*, 60, 1987.

Hassam, A. B., and J. D. Huba, Magnetohydrodynamic equations for systems with large Larmor radius, *Phys. Fluids, 31*, 318, 1988.

Huba, J. D., J. G. Lyon, and A. B. Hassam, Theory and simulation of the Rayleigh Taylor instability in the large Larmor radius limit, *Phys. Rev. Lett., 59*, 2971, 1987.

Krimigis, S. M., G. Haerendel, R. W. McEntire, G. Paschmann, and D. A. Bryant, The active magnetospheric particle tracers explorers (AMPTE) program, *Eos (Trans), 63*, 843, 1982.

Okada, S., K. Sato, and T. Sekiguchi, Behavior of laser produced plasma in a uniform magnetic field–plasma instabilities, *Japan J. Appl. Phys., 20*, 157, 1981.

Ripin, B. H., E. A. McLean, C. K. Manka, C. Pawley, J. A. Stamper, T. A. Peyser, A. N. Mostovych, J. Grun, A. B. Hassam, and J. D. Huba, Large Larmor radius interchange instability, *Phys. Rev. Lett., 59*, 2299, 1987.

Sgro, A. G., S. P. Gary, and D. S. Lemons, Expanding plasma structure and its evolution toward long wavelengths, *Phys. Fluids*, submitted, 1988.

Winske, D., Short wavelength modes on expanding plasma clouds, *J. Geophys. Res. 93*, 2539, 1988.

Winske, D., Development of flute modes on expanding plasma clouds, *Phys. Fluids*, submitted, 1989.

DISTRIBUTION

Dr. B. H. Ripin
Code 4732
Naval Res. Lab.
Washington, DC 20375

Dr. E. McLean
Code 4732
Naval Res. Lab.
Washington, DC 20375

Dr. J. Stamper
Code 4732
Naval Res. Lab.
Washington, DC 20375

Dr. Paul Bernhardt
Code 4780
Naval Res. Lab.
Washington, DC 20375

Dr. Walter Chesnut
SRI International
333 Ravenswood Ave.
Menlo Park, CA 94025

Dr. J. L. Sperling
JAYCOR
11011 Torreyana Road
P. O. Box 85154
San Diego, CA 92138

Dr. R. Stellingwerf
Mission Research Corp.
1720 Randolph Rd. S. E.
Albuquerque, NM 87106

Dr. R. Peterkin
Mission Research Corp.
1720 Randolph Rd. S. E.
Albuquerque, NM 87106

Dr. K. Hain
Maxwell S-Cubed Div.
1800 Diagonal Rd.
Alexandria, VA 22314

Dr. E. Hyman
SAIC
1710 Goodridge Dr.
McLean, VA 22102

Dr. J. Guillory
PRC
5850 Leesburg Pike # 23
Falls Church, VA 22041

Dr. L. Wittwer
RAAE
Defense Nuclear Agency
Washington, DC 20305

Dr. B. Prasad
RAAE
Defense Nuclear Agency
Washington, DC 20305

Director [2]
Attn: STTI
Defense Nuclear Agency
Washington, DC 20305-1000

Dr. R. W. Kilb
Mission Research Corp.
P. O. Box 719
Santa Barbara, CA 93102

Dr. W. W. White
Mission Research Corp.
P. O. Box 719
Santa Barbara, CA 93102

Dr. M. Hausman
Mission Research Corp.
P. O. Box 719
Santa Barbara, CA 93102

Dr. D. Sowle
Mission Research Corp.
P. O. Box 719
Santa Barbara, CA 93102

Prof. D. Papadopoulos
Astronomy Program
University of Maryland
College Park, MD 20742

Dr. J. D. Huba
Code 4780
Naval Res. Lab.
Washington, DC 20375

Dr. J. Lyon
Code 4780
Naval Res. Lab.
Washington, DC 20375

Dr. J. Giuliani
Code 4780
Naval Res. Lab.
Washington, DC 20375

Dr. S. Brecht
Berkeley Research Associates
P.O. Box 241
Berkeley, CA 94701

Dr. V. Thomas
Berkeley Research Associates
P.O. Box 241
Berkeley, CA 94701

Dr. H. Carl Fitz
Physical Research, Inc.
134 Holiday Ct., Suite 309
Annapolis, MD 21401

Dr. R. Armstrong
Mission Research Corp.
One Tara Blvd. Suite 302
Nashua, NH 03062

Defense Technical Information Center [2]
Cameron Station
Alexandrai, VA 22314

Dr. R. Henderson, W385
Director, JASON Program Office
The MITRE Corp.
7525 Colshire Dr.
McLeam, VA 22102

DASIAC
815 State St.
P.O. Drawer QQ
Santa Barbara, CA 93102

Dr. J. Kindel
MRC
127 Eastgate #20800
Los Alamos, NM 87544

Dr. T. Mazurek
Mission Research Corp.
P. O. Box 719
Santa Barbara, CA 93102

Dr. C. Longmire
Mission Research Corp.
P. O. Box 719
Santa Barbara, CA 93102

Dr. E. Witt
Mission Research Corp.
P. O. Box 719
Santa Barbara, CA 93102

Dr. J. R. Thompson
Austin Research Associates
1901 Rutland Dr.
Austin, TX 78758

Dr. J. M. Cornwall
Dept. of Physics
UCLA
Los Angeles, CA 90024

Dr. D. Hammer
Laboratory for Plasma Studies
809 Upson Hall
Cornell University
Ithaca, NY 14853

Dr. C. Prettie
Berkeley Research Associates
P.O. Box 241
Berkeley, CA 94701

Dr. J. Workman
Berkeley Research Associates
P.O. Box 241
Berkeley, CA 94701

Dr. D. Simons
ESS-7
MS D466

Dr. D. Sappenfield
ESS-7
MS D466

Dr. G. Smith
ESS-DOT
MS D446

Dr. M. Pongratz
ESS-DOT
MS D446